methane

MDPI

Communication

Methane to Methanol Conversion Using Proton-Exchange Membrane Fuel Cells and PdAu/Antimony-Doped Tin Oxide Nanomaterials

Victória A. Maia [1], Julio Nandenha [1], Marlon H. Gonçalves [1,2], Rodrigo F. B. de Souza [1] and Almir O. Neto [1,*]

[1] Instituto de Pesquisas Energéticas e Nucleares, IPEN-CNEN/SP, Cidade Universitária, Av. Professor Lineu Prestes, 2242, São Paulo 05508-900, Brazil; victoriaamaia@usp.br (V.A.M.); nandenhajb@yahoo.com.br (J.N.); marlondeholanda@gmail.com (M.H.G.); souza.rfb@gmail.com (R.F.B.d.S.)
[2] Faculdade Oswaldo Cruz R. Brg. Galvão, 540-Barra Funda, São Paulo 01151-000, Brazil
* Correspondence: aolivei@usp.br

Abstract: This study investigates the use of Au-doped Pd anodic electrocatalysts on ATO support for the conversion of methane to methanol. The study uses cyclic voltammetry, in situ Raman spectra, polarization curves, and FTIR analysis to determine the optimal composition of gold and palladium for enhancing the conversion process. The results demonstrate the potential for utilizing methane as a feedstock for producing sustainable energy sources. The $Pd_{75}Au_{25}$/ATO electrode exhibited the highest OCP value, and $Pd_{50}Au_{50}$/ATO had the highest methanol production value at a potential of 0.05 V. Therefore, it can be concluded that an optimal composition of gold and palladium exists to enhance the conversion of methane to methanol. The findings contribute to the development of efficient and sustainable energy sources, highlighting the importance of exploring alternative ways to produce methanol.

Keywords: methane conversion; fuel cell; methanol; PEM; PdAu/ATO

check for updates

Citation: Maia, V.A.; Nandenha, J.; Gonçalves, M.H.; de Souza, R.F.B.; Neto, A.O. Methane to Methanol Conversion Using Proton-Exchange Membrane Fuel Cells and PdAu/Antimony-Doped Tin Oxide Nanomaterials. *Methane* **2023**, *2*, 252–264. https://doi.org/10.3390/methane2030017

Academic Editor: Patrick Da Costa

Received: 19 April 2023
Revised: 13 June 2023
Accepted: 21 June 2023
Published: 25 June 2023

Copyright: © 2023 by the authors. Licensee MDPI, Basel, Switzerland. This article is an open access article distributed under the terms and conditions of the Creative Commons Attribution (CC BY) license (https://creativecommons.org/licenses/by/4.0/).

1. Introduction

Methane is a widely available and inexpensive source of energy, but its combustion for energy production releases CO_2, contributing to climate change [1]. Therefore, researchers are exploring alternative methods to convert methane into chemicals like methanol, which can be utilized as a clean fuel and has diverse industrial applications [2]. Various techniques have been developed for methane conversion, including homogeneous and heterogeneous catalysis, photocatalysis [3], biocatalysis, plasma technologies, and electrochemical processes [4–7]. Among these, electrochemical processes have shown promise for converting methane into methanol under mild conditions and generating electricity [8–11].

To co-generate chemicals and electricity, one possible approach is to use a polymer electrolyte fuel cell as a reactor for converting methane into methanol and formates [11,12]. However, this conversion is challenging due to the high strength of the C-H bond in methane (434 $kJ \cdot mol^{-1}$) and its low polarizability because of its regular tetrahedron conformation [13]. Therefore, the process involves oxidizing methane through a non-faradaic reaction, which activates methane using more reactive species generated via faradaic processes, such as reactive oxygen species (ROS) from water activation. The significance of water activation in transferring oxygen to hydrocarbon molecules to produce methanol has been emphasized by researchers [14–16].

To achieve this conversion, catalysts with specific characteristics are required. One of the key requirements is for the catalysts to have a bifunctional effect [17–19], that is, to be able to adsorb methane and activate water molecules. While transition metal oxides are commonly used catalysts, researchers have been exploring alternative catalysts, such as platinum and palladium, which have shown promising results in methane oxidation to methanol [11,20].

Palladium- and gold-supported carbon materials, such as carbon nanotubes, activated carbon, and reduced graphene oxide [21,22], have been identified as effective catalysts for this process. Pd-Au nanoparticles have been used as active centers, and their catalytic activity can be improved by supporting them on functionalized carbon nanotubes [23]. In addition, gold's affinity for oxygen can facilitate the breakdown of hydrogen peroxide into OH•, which activates the C-H bond [21,24,25].

On the other hand, the oxygenated species produced can also attack the catalyst support, typically carbon, which affects the reactor's durability. Recent studies have explored the use of metallic oxides like TiO_2 and antimony-doped tin oxide (ATO) as catalyst support to improve catalyst stability [26–28]. In this context, this study investigated the conversion of methane to methanol in a polymer electrolyte fuel cell using Au-doped palladium anodic electrocatalysts in different proportions on an ATO (antimony-doped tin oxide) support. ATO was selected as the support because it promotes the formation of reactive oxygen species, and has good electrical conductivity and corrosion resistance, making it a promising catalyst support option for the methane-to-methanol reaction [29–32].

2. Results

Figure 1 presents microscopy images and nanoparticle size distribution histograms for Au/ATO, Pd/ATO, and PdAu/ATO with varying ratios. The average nanoparticle size ranges from 12 to 19 nm, with the smallest size (12 nm) observed in the Pd/ATO catalyst and the largest size (19 nm) observed in the $Pd_{50}Au_{50}$/ATO catalyst. Additionally, the images show that the nanoparticles are not well dispersed on the support and tend to agglomerate. The ATO support's ability has been observed in other catalytic materials in the literature [29–35].

X-ray diffraction (XRD), as shown in Figure 2a, was utilized to characterize the chemical structures of a series of Pd/ATO, Au/ATO, and PdAu/ATO samples. The peaks observed at $2\theta \approx 26°$, 33°, 38°, 51°, 54°, 62°, and 64° correspond to the characteristic diffraction peaks of $SnO_2.Sb_2O_5$ (JCPDS# 88-2348). The palladium and gold peaks appear discreetly in comparison. Based on the diffraction pattern with intensity normalized by the logarithmic function (Figure 2b), it was possible to clearly observe the characteristic peaks of Pd and Au. The Pd-related peaks at $2\theta \approx 38°$, 49°, and 66° are associated with the crystalline planes (111), (200), (220), and (311), according to (JCPDS# 89-4897), which reveals a face-centered cubic (FCC) structure for Pd/ATO. The relative intensities of Pd and ATO are still discrete, even when normalized on a logarithmic scale, reflecting the smaller particle size compared to the other materials.

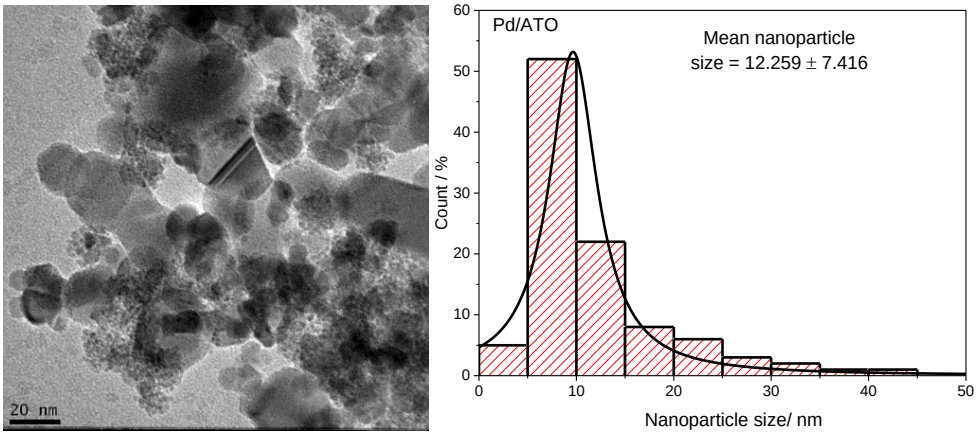

(a)Pd/ATO

Figure 1. *Cont.*

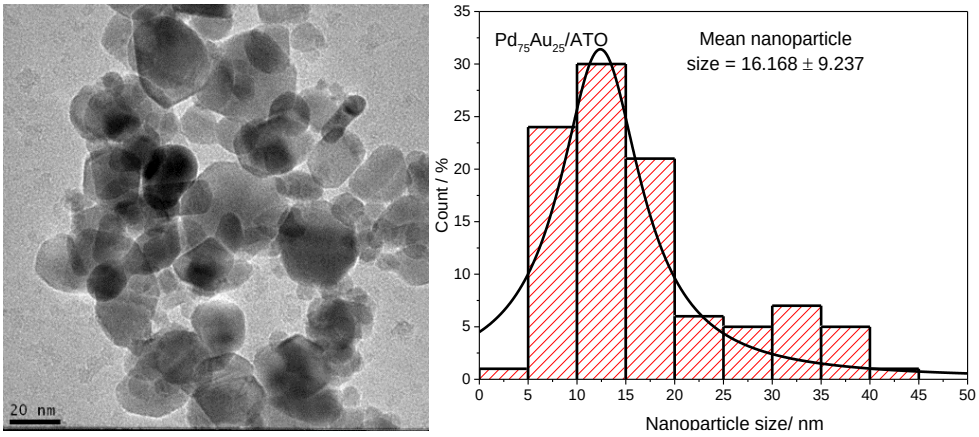

(b)$Pd_{75}Au_{25}$/ATO

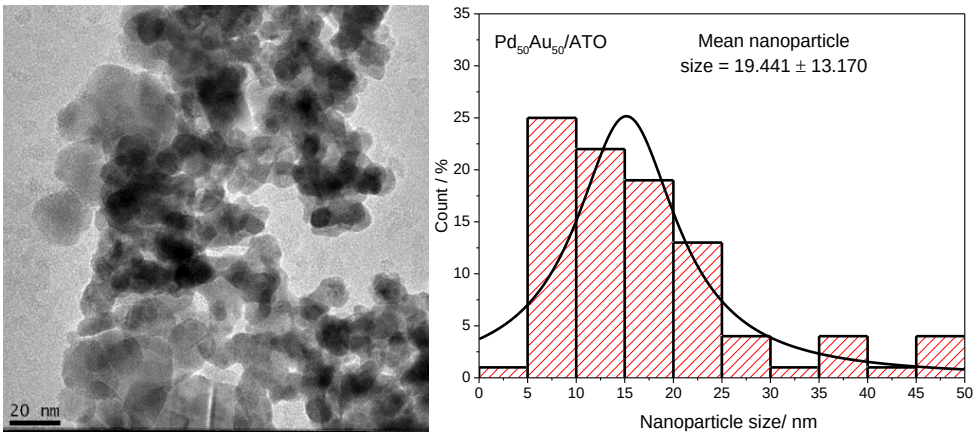

(c)$Pd_{50}Au_{50}$/ATO

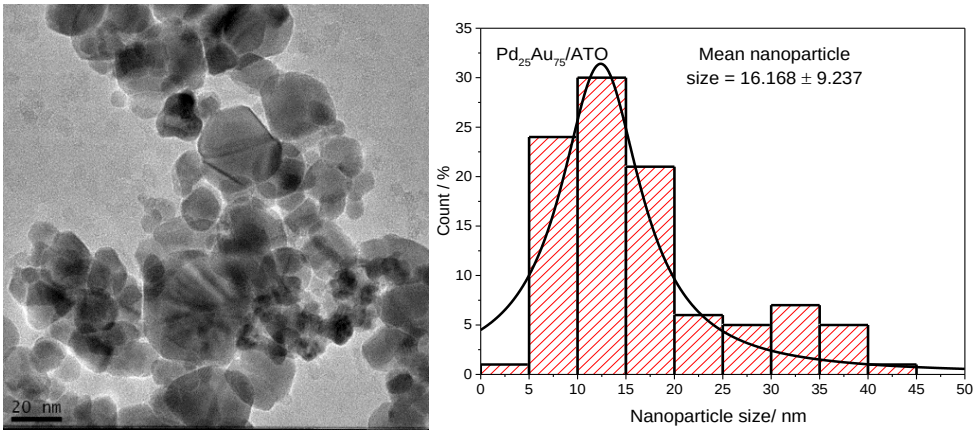

(d)$Pd_{25}Au_{75/}$ATO

Figure 1. *Cont.*

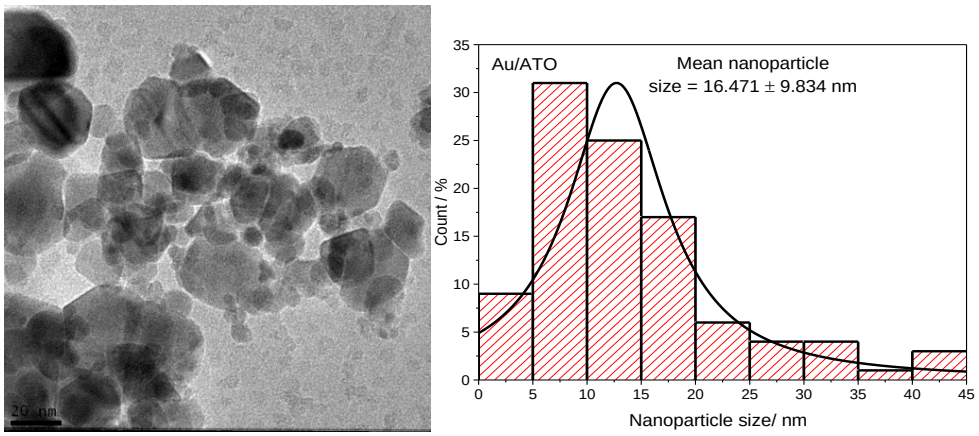

(e) Au/ATO

Figure 1. TEM micrographs and histograms of nanoparticle size distributions in, (**a**) Pd/ATO, (**b**) $Pd_{75}Au_{25}$/ATO, (**c**) $Pd_{50}Au_{50}$/ATO, (**d**) $Pd_{25}Au_{75}$/ATO and (**e**) Au/ATO.

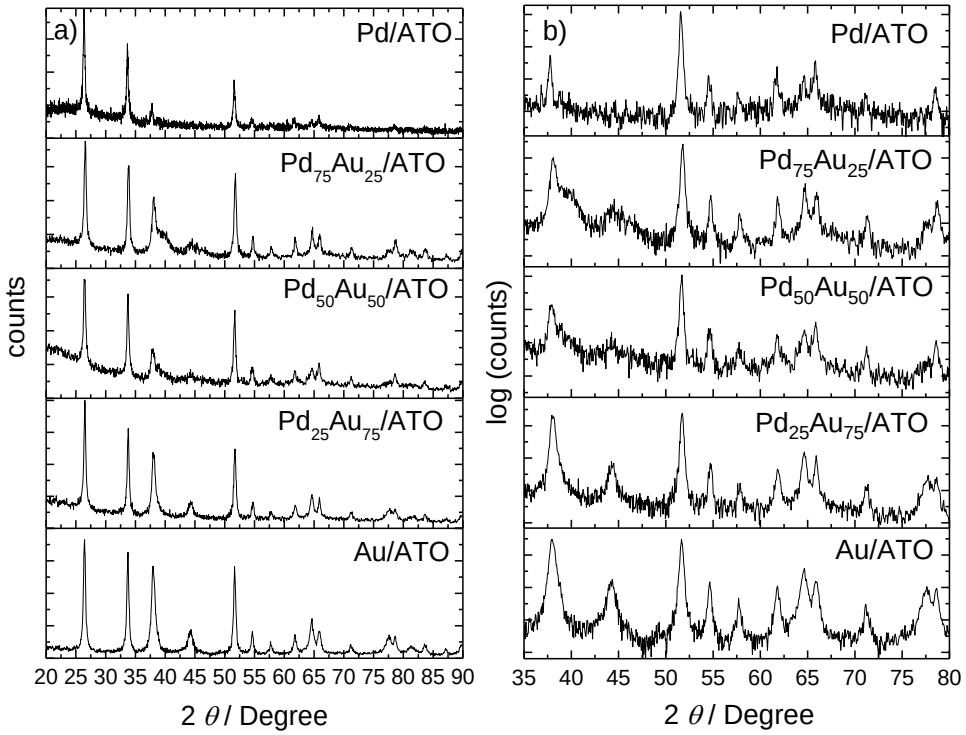

Figure 2. X-ray diffractogram (XRD) patterns of Au/ATO, Pd/ATO, and PdAu/ATO in different ratios. (**b**) Logarithm of the intensities of the diffractograms in (**a**).

Two small reflection peaks were observed at $2\theta \approx 38.1^\circ$ and 44.4°, corresponding to the (1 1 1) and (2 0 0) planes of face-centered cubic-structured Au (JCPDS no. 89-3697). The peaks relative to the (2 2 0) and (3 1 1) planes at $2\theta \approx 64^\circ$ and 77°, respectively, appear convoluted with the peaks of Pd and tin oxide. It is noteworthy that the peak with the (3 1 1) plane stands out.

The cyclic voltammetry of PdAu materials, in different molar ratios in 1.0 mol L^{-1} NaOH aqueous solution (scan rate v = 10 mV s^{-1}), is presented in Figure 3a. In the materials containing Pd, it is possible to observe in the region of -0.85 and -0.5 V the peaks corresponding to hydrogen adsorption and desorption [36], the Pd/ATO electrode presenting the oxide reduction (-0.4 V), and oxide formation (0.05 V). The PdAu/ATO

electrodes show a shift in the peak positions for the hydrogen adsorption–desorption, compared to Pd/ATO, which indicates the electronic modification of Pd atoms by Au [37].

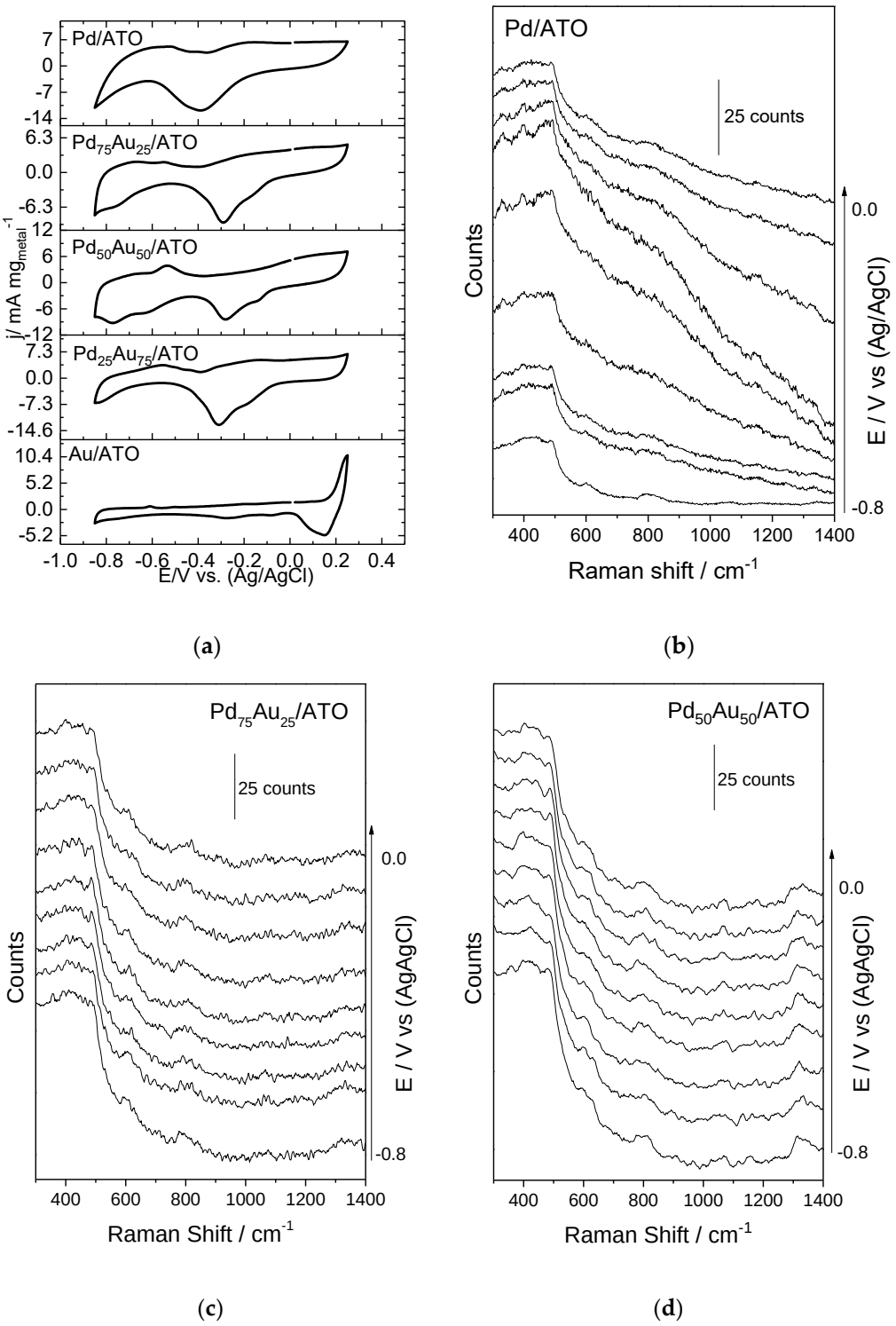

Figure 3. *Cont.*

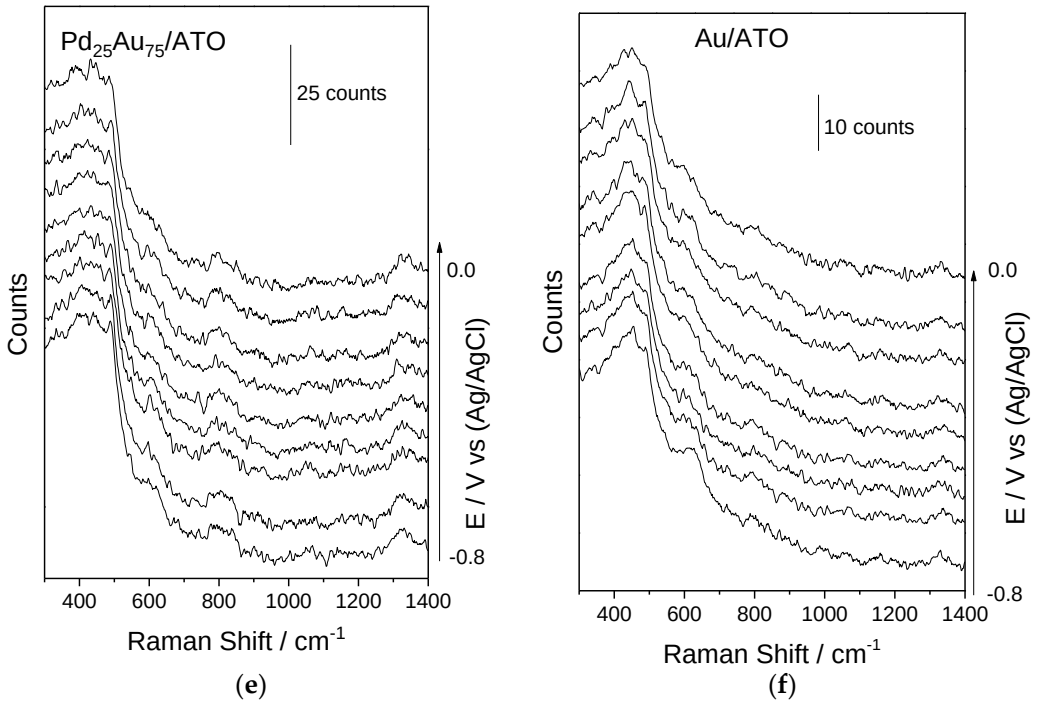

Figure 3. (**a**) Cyclic voltammetry (CV) of Au/ATO, Pd/ATO, and PdAu/ATO in different ratios (scan rate v = 10 mV s^{-1}) in 1 mol L^{-1} NaOH aqueous solution. (**b**–**f**) Spectra of in situ Raman-assisted electrochemical measurements collected at different potentials in NaOH 1.0 mol L^{-1}.

The presence of gold sites near palladium sites can alter the chemical environment and shift the hydrogen desorption potential to less negative values with an increase in the gold content in the material (−0.55, −0.57, and −0.59 V for $Pd_{75}Au_{25}$/ATO, $Pd_{50}Au_{50}$/ATO, and $Pd_{25}Au_{75}$/ATO, respectively). In order to complement and expand the observations from cyclic voltammetry, in situ Raman spectra of the Pd-Au materials were measured (Figure 3b). In all of the spectra, the characteristic bands of SnO_2 are observed at approximately 486, 602, and 780–793 cm^{-1}, corresponding to the active bands of SnO_2 Eg, A_1g, and B_2g, respectively [38,39]. Additionally, a band centered at 639 cm^{-1}, corresponding to the bending of the PdO-H bond [40], indicates the oxidation of Pd as a function of potential in the Pd/ATO catalyst.

For all materials containing gold, it is possible to observe a feature at potentials less negative than −0.4 V, which is assigned to the Au-O stretching vibration of Au oxide and appears at approximately 559 cm^{-1} [41], and this potential is shifted for more negative values as the gold content increases. The 635 cm^{-1} band refers to the Au-O and Au-OOH vibrations [42], and this band decreases with the addition of Pd. The band observed at 602 cm^{-1} in SnO_2 overlapped with this band, while distinct bands were observed at 794, 974, and 1166 cm^{-1}, which can be attributed to Nafion [43].

The polarization curves (Figure 4) of the partial oxidation of methane in a polymer electrolyte reactor and the measured open circuit potential (OCP) values range between 0.3 and 0.5 V, which are comparable to those reported in the other literature [3,29]. The Pd75Au25/ATO electrode exhibits the highest OCP value, while the Au/ATO electrode has the lowest, indicating that the synergy between Pd and Au increases the OCP value compared to that of Pd or Au alone. The Au/ATO and $Pd_{25}Au_{75}$/ATO electrodes have the same OCP value, but the power density of $Pd_{25}Au_{75}$/ATO is 0.9 mW/cm^2, which is higher than that of Au/ATO (0.49 mW/cm^2). The results indicate that the addition of gold to palladium can favor the generation of methane oxidation products through reactive oxygen species, which in turn can be oxidized by Pd. Since the oxidation potentials of methanol and formic acid are lower than the water activation potential, they can lead to an increase in the open circuit potential.

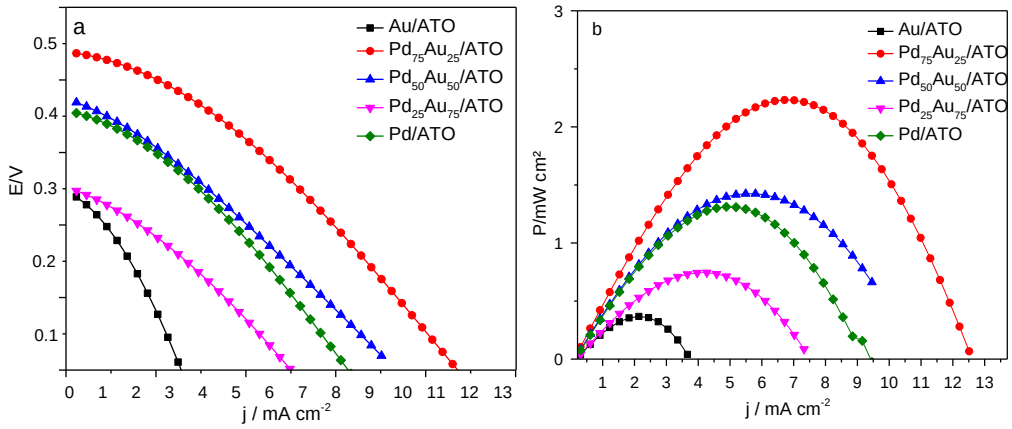

Figure 4. (**a**) Polarization curves of ATO-supported PdAu materials in different compositions. (**b**) Power density curves.

The FTIR analysis (Figure 5) displays the spectra of aliquots collected from the reactor effluent every 100 mV for 5 min in a 1.0 mol L^{-1} NaOH solution, with a methane flow rate adjusted to 100 mL min^{-1} for all of the catalysts. The obtained spectra exhibit a characteristic methane band at ~1304 cm^{-1}, corresponding to CH_4 dissolving in water [44,45]. Methanol formation can be identified by specific bands that appear at 1033, 1077, and 1082 cm^{-1} [46], although they are subtle and present in all materials. Additionally, a band centered at ~1342 cm^{-1} corresponding to the ν(COO) of formate in the solution [47] is visible in all of the materials. This band may indicate that the process is leading to more oxidized products of methane than methanol. The presence of formic acid peaks in the gold-content materials already at the OCP indicates the production of more oxidized products even at the lowest possible overpotentials at the anode.

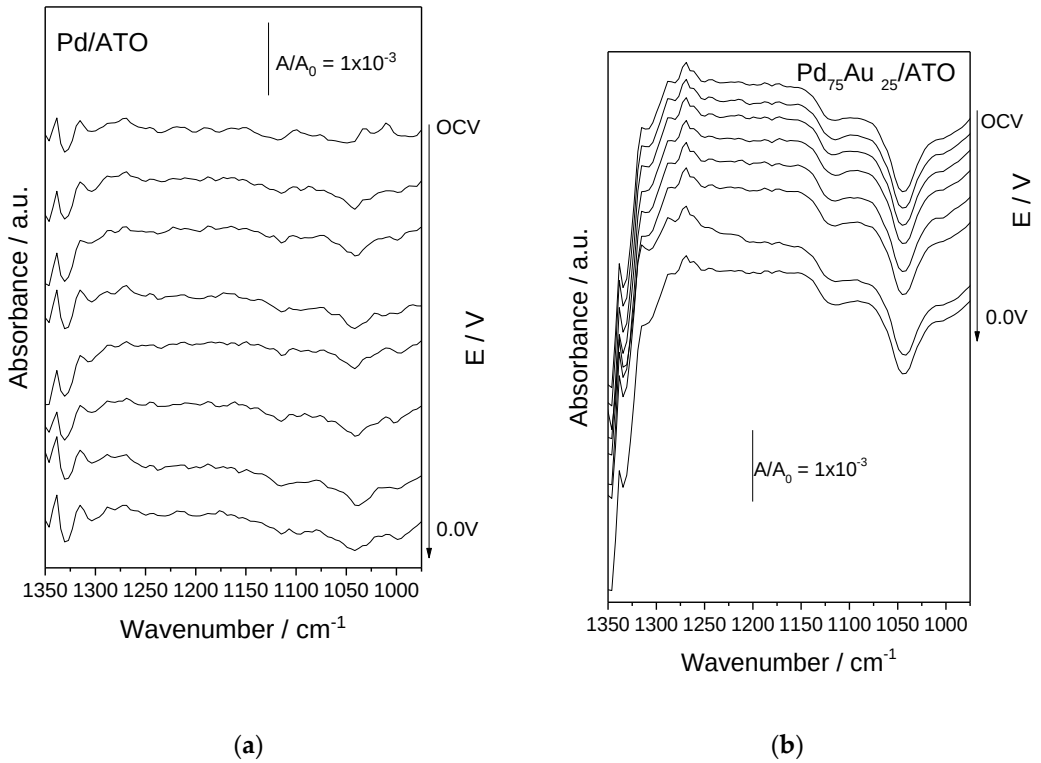

(**a**) (**b**)

Figure 5. *Cont.*

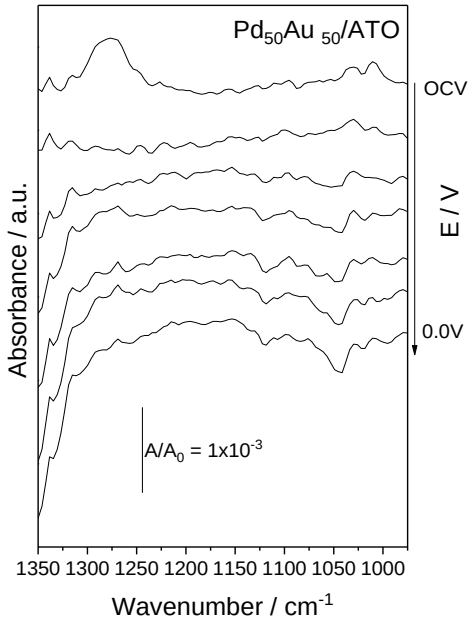

(**c**)

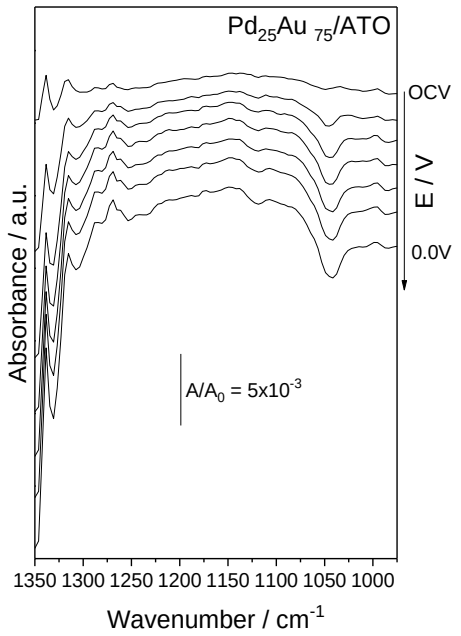

(**d**)

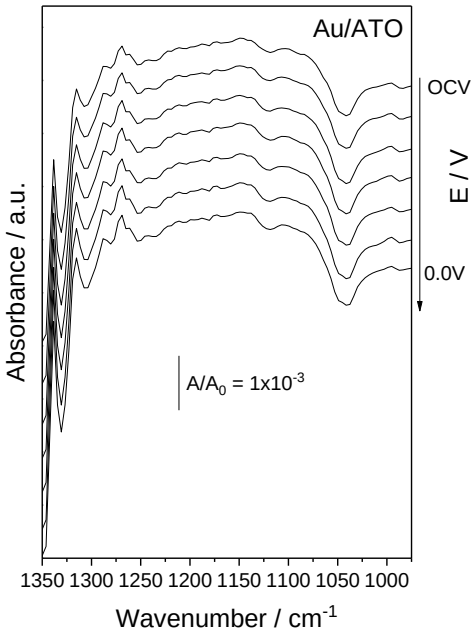

(**e**)

Figure 5. Spectra of FTIR aliquots collected from the reactor effluent every 100 mV for 5 min in presence of NaOH 1.0 mol L $^{-1}$, with methane flow adjusted to 100 mL min $^{-1}$ for (**a**) Pd/ATO, (**b**) $Pd_{75}Au_{25}$/ATO, (**c**) $Pd_{50}Au_{50}$/ATO, (**d**) $Pd_{25}Au_{75}$/ATO and (**e**) Au/ATO in potentials of −0.4; −0.3; −0.2; −0.1 and 0.0 V.

The collected effluent from the reactor was also used to quantify the methanol produced via HPLC, and this value was converted and reported as the rate of reaction (Equation (1)).

$$r = ([methanol])/(V*time) \quad (1)$$

Figure 6 reports the rate of reaction for palladium- and gold-based materials. The data show that $Pd_{50}Au_{50}$/ATO has the highest methanol production value at a potential of −0.05 V, outperforming all of the other materials and potentials. These results indicate that an optimal composition of gold and palladium exists to enhance the conversion of methane to methanol. The combination of gold's oxophilic nature [21,22], which facilitates water activation, with PdO's carbophilic ability [11], and the balance between the two types of sites, favors the pathway of methane conversion to methanol.

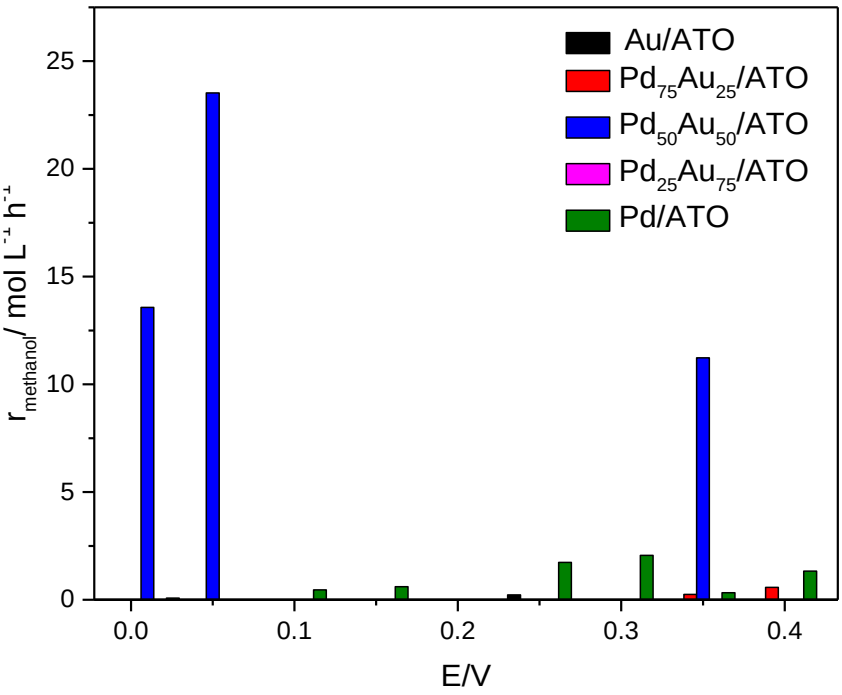

Figure 6. Rate reaction of Au/ATO, Pd/ATO, and PdAu/ATO in different potentials.

The observed results for Pd50Au50/ATO are up to 3 times higher than those reported in the literature for PdNi (~8 mol L^{-1} h^{-1}) [29]. There is no formation of methanol in measurable quantities for $Pd_{25}Au_{75}$/ATO.

3. Materials and Methods

The PdAu/ATO materials were synthesized using the sodium borohydride reduction method [28] with varying ratios. To prepare each material, a solution of ultrapure water and isopropanol (50/50 v/v) was mixed with a specific amount of ATO support (Sb_2O_5•SnO_2 Aldrich) in an ultrasonic bath for 15 min. Subsequently, 20% of metallic precursors $Pd(NO_3)_2$•2 H_2O (Aldrich) and $HAuCl_4$•3 H_2O (Aldrich) was added in different ratios. In this medium, NaBH4 (Aldrich) was added to a 10 mL 0.01 mol L^{-1} NaOH solution with an excess of 5:1 in relation to the metals, and stirring was maintained for 30 min. The resulting material was then washed and filtered using 4 L of ultrapure water (18 MΩ cm^{-1}).

The morphology of PdAu/ATO (nanoparticle size and general aspects) was investigated using transmission electronical microscopy (TEM) via JEOL JEM-2100, operated at 200 keV. For the histogram and the calculation of the average size, 300 nanoparticles of each catalyst were calculated using the ImageJ software package. The crystalline structure of the materials was analyzed using a diffractometer (Rigaku–Miniflex II) at Cu/kα λ = 0.154 nm, with 2θ ranging from 20 to 90°, with a scan speed of 2° min^{-1}, operating at 40 kV. The analyzed XRD standards were compared with those of JCPDS (Joint Committee on Powder Diffraction).

The electrochemical experiments were observed via cyclic voltammetry (CV) performed on a three-electrode cell, connected to a potentiostat/galvanostat (PGSTAT 302 N,

Autolab®), with PdAu/ATO as the working electrode, a 2 cm^2 Pt plate as the counter electrode, and a commercial Ag/AgCl electrode (3.0 mol L^{-1} solution) as the reference electrode, all in a single compartment cell. The Raman in situ spectra were analyzed using a Raman Micro Spectrometer—Horiba—with a 785 nm laser and the same single compartment cell used in the CV experiments.

A PEM fuel cell unit was used in this work, similar to that applied in previous studies [29,30]. Five different membrane electrode assemblies (MEAs) of anode/electrolyte/cathode were constructed. Different 1 mg per cm^2 of metals (Pd:Au) were used as the anode, a membrane of Nafion® 117 (DuPont®) treated with KOH was used as the electrolyte, and 1 mg of Pt/C—BASF (20% *w*/*w*) was used as the cathode. The ink contains the catalyst with 30% of the mass of a solution of Nafion® D-520 (Aldrich) and isopropanol. The anodes were prepared by brushing the ink on carbon cloth treated with PTFE [31,32]. The conditions of the fuel cell were fed with a mixture of methane (100 mL min^{-1}) and NaOH 1 mol L^{-1} at a (1 mL min^{-1}) supply at the anode, while the cathode was supplied with a humidified O_2 bottle at a temperature of 85 °C with a flow rate of 400 mL min^{-1}. The temperature measurement in the cell was 45 °C. For the application of currents and potentials to the cell, a potentiostat/galvanostat (PGSTAT 302 N, Autolab®) was used.

The reaction products were collected from the reactor every 5 min in the open circuit potential (OCP) until 0.0 V and analyzed using infrared (IR) spectroscopy performed on a Nicolett® 6700 with ATR Miracle (Pike) accessory, diamond/ZnSe crystal, and a detector of MCT, as well as high-performance liquid chromatography (HPLC) (YL9100) with a UV/Vis detector at 225 nm and flow of 0.8 mL min^{-1} of 50% water, 40% acetonitrile, and 10% buffer solution in an isocratic run on a C18 (Phenomenex Luna 5 µm, 250 × 4.6 nm). The calibration curve presents the following linear equation: peak area = 0.29574 + 0.00979 [methanol] and presents r^2 = 0.994.

4. Conclusions

This study examined the conversion of methane to methanol in a polymer electrolyte fuel cell using Au-doped palladium anodic electrocatalysts in different proportions on an ATO support. The cyclic voltammetry and in situ Raman spectra of the Pd-Au materials were measured to observe the electronic modification of Pd atoms by Au. The polarization curves of the partial oxidation of methane in a polymer electrolyte reactor and the measured open circuit potential values were also studied. The results showed that the $Pd_{75}Au_{25}$/ATO electrode exhibited the highest OCP value, probably due to gold promoting the formation of methane oxidation products through reactive oxygen species, which can subsequently be oxidized by Pd. Due to the lower oxidation potentials of methanol and formic acid compared to the water activation potential, their presence can result in an increase in the open circuit potential. The optimal activation of water in conjunction with Pd sites provided by the $Pd_{50}Au_{50}$/ATO material led to the highest methanol production. Therefore, it can be concluded that an optimal composition of gold and palladium exists to enhance the conversion of methane to methanol. This study contributes to the development of efficient and sustainable energy sources by utilizing methane, a potent greenhouse gas, as a feedstock for producing methanol.

Author Contributions: Conceptualization, A.O.N. and R.F.B.d.S.; methodology, A.O.N. and R.F.B.d.S.; validation, M.H.G. and V.A.M.; formal analysis, V.A.M.; investigation, V.A.M.; resources, V.A.M.; writing—original draft preparation, V.A.M.; writing—review and editing, J.N., R.F.B.d.S. and A.O.N.; supervision, A.O.N. and R.F.B.d.S.; project administration, A.O.N.; funding acquisition, A.O.N. All authors have read and agreed to the published version of the manuscript.

Funding: FAPEAM (N.012/2021–POSGFE), CAPES, CNPQ (302709/2020-7, 407967/2022-2), and FAPESP (2017/11937-4).

Institutional Review Board Statement: Not applicable.

Informed Consent Statement: Not applicable.

Data Availability Statement: Individuals interested in accessing the data may request them from the authors by providing a justification, and the authors will provide them at their convenience.

Conflicts of Interest: The authors declare no conflict of interest.

References

1. Blanco, H.; Nijs, W.; Ruf, J.; Faaij, A. Potential of Power-to-Methane in the EU energy transition to a low carbon system using cost optimization. *Appl. Energy* **2018**, *232*, 323–340. [CrossRef]
2. Jang, J.; Shen, K.; Morales-Guio, C.G. Electrochemical Direct Partial Oxidation of Methane to Methanol. *Joule* **2019**, *3*, 2589–2593. [CrossRef]
3. Premachandra, D.; Heagy, M.D. Morphology-Controlled WO3 for the Photocatalytic Oxidation of Methane to Methanol in Mild Conditions. *Methane* **2023**, *2*, 103–112. [CrossRef]
4. de Souza, R.F.B.; Florio, D.Z.; Antolini, E.; Neto, A.O. Partial Methane Oxidation in Fuel Cell-Type Reactors for Co-Generation of Energy and Chemicals: A Short Review. *Catalysts* **2022**, *12*, 217. [CrossRef]
5. Ikuno, T.; Zheng, J.; Vjunov, A.; Sanchez-Sanchez, M.; Ortuño, M.A.; Pahls, D.R.; Fulton, J.L.; Camaioni, D.M.; Li, Z.; Ray, D.; et al. Methane Oxidation to Methanol Catalyzed by Cu-Oxo Clusters Stabilized in NU-1000 Metal–Organic Framework. *J. Am. Chem. Soc.* **2017**, *139*, 10294–10301. [CrossRef]
6. Sushkevich, V.L.; van Bokhoven, J.A. Kinetic study and effect of water on methane oxidation to methanol over copper-exchanged mordenite. *Catal. Sci. Technol.* **2020**, *10*, 382–390. [CrossRef]
7. Dalton, H. The Leeuwenhoek Lecture 2000 The natural and unnatural history of methane-oxidizing bacteria. *Philos. Trans. R. Soc. Lond. B* **2005**, *360*, 1207–1222. [CrossRef]
8. Otsuka, K.; Yamanaka, I. Electrochemical cells as reactors for selective oxygenation of hydrocarbons at low temperature. *Catal. Today* **1998**, *41*, 311–325. [CrossRef]
9. Lee, B.; Hibino, T. Efficient and selective formation of methanol from methane in a fuel cell-type reactor. *J. Catal.* **2011**, *279*, 233–240. [CrossRef]
10. Tomita, A.; Nakajima, J.; Hibino, T. Direct Oxidation of Methane to Methanol at Low Temperature and Pressure in an Electrochemical Fuel Cell. *Angew. Chem. Int. Ed.* **2008**, *47*, 1462–1464. [CrossRef]
11. Santos, M.C.L.; Nunes, L.C.; Silva, L.M.G.; Ramos, A.S.; Fonseca, F.C.; de Souza, R.F.B.; Neto, A.O. Direct Alkaline Anion Exchange Membrane Fuel Cell to Converting Methane into Methanol. *ChemistrySelect* **2019**, *4*, 11430–11434. [CrossRef]
12. Henrique, R.S.; De Souza, R.F.B.; Silva, J.C.M.; Ayoub, J.M.S.; Piasentin, R.M.; Linardi, M.; Spinacé, E.V.; Santos, M.C.; Neto, A.O. Preparation of Pt/C-In_2O_3.SnO_2 Electrocatalysts by Borohydride Reduction Process for Ethanol Electro-Oxidation. *Int. J. Electrochem. Sci.* **2012**, *7*, 2036–2046.
13. Jiang, H.; Zhang, L.; Han, Z.; Tang, Y.; Sun, Y.; Wan, P.; Chen, Y.; Argyle, M.D.; Fan, M. Direct conversion of methane to methanol by electrochemical methods. *Green Energy Environ.* **2021**, *7*, 1132–1142. [CrossRef]
14. Cook, R.L.; Sammells, A.F. Ambient Temperature Methane Activation to Condensed Species under Cathodic Conditions. *J. Electrochem. Soc.* **1990**, *137*, 2007–2008. [CrossRef]
15. Garcia, L.M.S.; Rajak, S.; Chair, K.; Godoy, C.M.; Silva, A.J.; Gomes, P.V.R.; Sanches, E.A.; Ramos, A.S.; De Souza, R.F.B.; Duong, A.; et al. Conversion of Methane into Methanol Using the [6,6′-(2,2′-Bipyridine-6,6′-Diyl)bis(1,3,5-Triazine-2,4-Diamine)](Nitrato-O)Coppe r(II) Complex in a Solid Electrolyte Reactor Fuel Cell Type. *ACS Omega* **2020**, *5*, 16003–16009. [CrossRef]
16. Ramos, A.S.; Santos, M.C.L.; Godoi, C.M.; Neto, A.O.; De Souza, R.F.B. Obtaining C2 and C3 Products from Methane Using Pd/C as Anode in a Solid Fuel Cell-type Electrolyte Reactor. *ChemCatChem* **2020**, *12*, 4517–4521. [CrossRef]
17. Antzara, A.; Heracleous, E.; Silvester, L.; Bukur, D.B.; Lemonidou, A.A. Activity study of NiO-based oxygen carriers in chemical looping steam methane reforming. *Catal. Today* **2016**, *272*, 32–41. [CrossRef]
18. Wang, S.; Itoh, T.; Fujimori, T.; de Castro, M.M.; Silvestre-Albero, A.; Rodríguez-Reinoso, F.; Ohba, T.; Kanoh, H.; Endo, M.; Kaneko, K. Formation of COx-Free H_2 and Cup-Stacked Carbon Nanotubes over Nano-Ni Dispersed Single Wall Carbon Nanohorns. *Langmuir* **2012**, *28*, 7564–7571. [CrossRef]
19. Jafarian, M.; Mahjani, M.G.; Heli, H.; Gobal, F.; Heydarpoor, M. Electrocatalytic oxidation of methane at nickel hydroxide modified nickel electrode in alkaline solution. *Electrochem. Commun.* **2003**, *5*, 184–188. [CrossRef]
20. Hsieh, S.; Chen, K. Anodic oxidation of methane. *J. Electrochem. Soc.* **1977**, *124*, 1171. [CrossRef]
21. He, Y.; Luan, C.; Fang, Y.; Feng, X.; Peng, X.; Yang, G.; Tsubaki, N. Low-temperature direct conversion of methane to methanol over carbon materials supported Pd-Au nanoparticles. *Catal. Today* **2020**, *339*, 48–53. [CrossRef]

22. Wang, B.; Tao, L.; Cheng, Y.; Yang, F.; Jin, Y.; Zhou, C.; Yu, H.; Yang, Y. Electrocatalytic Oxidation of Small Molecule Alcohols over Pt, Pd, and Au Catalysts: The Effect of Alcohol's Hydrogen Bond Donation Ability and Molecular Structure Properties. *Catalysts* **2019**, *9*, 387. [CrossRef]
23. Serra-Maia, R.; Michel, F.M.; Kang, Y.; Stach, E.A. Decomposition of Hydrogen Peroxide Catalyzed by AuPd Nanocatalysts during Methane Oxidation to Methanol. *ACS Catal.* **2020**, *10*, 5115–5123. [CrossRef]
24. He, Y.; Liang, J.; Imai, Y.; Ueda, K.; Li, H.; Guo, X.; Yang, G.; Yoneyama, Y.; Tsubaki, N. Highly selective synthesis of methanol from methane over carbon materials supported Pd-Au nanoparticles under mild conditions. *Catal. Today* **2020**, *352*, 104–110. [CrossRef]
25. McVicker, R.; Agarwal, N.; Freakley, S.J.; He, Q.; Althahban, S.; Taylor, S.H.; Kiely, C.J.; Hutchings, G.J. Low temperature selective oxidation of methane using gold-palladium colloids. *Catal. Today* **2020**, *342*, 32–38. [CrossRef]
26. Sun, L.; Liu, Z.; Bao, Y.; Li, H.; Bao, W. High-activity of Pd catalyst supported on antimony tin oxide for hydrogen peroxide electroreduction. *Int. J. Mater. Res.* **2014**, *105*, 584–587. [CrossRef]
27. de Moura Souza, F.; de Souza, R.F.B.; Batista, B.L.; Santos, M.C.D.; Fonseca, F.C.; Neto, A.O.; Nandenha, J. Methane activation at low temperature in an acidic electrolyte using PdAu/C, PdCu/C, and $PdTiO_2$/C electrocatalysts for PEMFC. *Res. Chem. Intermed.* **2020**, *46*, 2481–2496. [CrossRef]
28. Piasentin, R.M.; Spinacé, E.V.; Tusi, M.M.; Neto, A.O. Preparation of PdPtSn/C-Sb_2O_5. SnO_2 electrocatalysts by borohydride reduction for ethanol electro-oxidation in alkaline medium. *Int. J. Electrochem. Sci.* **2011**, *6*, 2255–2263.
29. Coelho, J.F.; Filho, N.G.P.; Gutierrez, I.M.; Godoi, C.M.; Gomes, P.V.R.; Zambiazi, P.J.; de Souza, R.F.B.; Neto, A.O. Methane-to-methanol conversion and power co-generation on palladium: Nickel supported on antimony tin oxide catalysts in a polymeric electrolyte reactor-fuel cell (PER-FC). Res. *Chem. Intermed.* **2022**, *48*, 5155–5168. [CrossRef]
30. Godoi, C.M.; Santos, M.C.L.; Silva, A.J.; Tagomori, T.L.; Ramos, A.S.; de Souza, R.F.B.; Neto, A.O. Methane conversion to higher value-added product and energy co-generation using anodes OF PdCu/C in a solid electrolyte reactor: Alkaline fuel cell type monitored by differential mass spectroscopy. *Res. Chem. Intermed.* **2021**, *47*, 743–757. [CrossRef]
31. Antoniassi, R.M.; Otubo, L.; Vaz, J.M.; Neto, A.O.; Spinacé, E.V. Synthesis of Pt nanoparticles with preferential (100) orientation directly on the carbon support for Direct Ethanol Fuel Cell. *J. Catal.* **2016**, *342*, 67–74. [CrossRef]
32. Ribeiro, V.A.; Correa, O.V.; Neto, A.O.; Linardi, M.; Spinacé, E.V. Preparation of PtRuNi/C electrocatalysts by an alcohol-reduction process for electro-oxidation of methanol. *Appl. Catal.* **2010**, *372*, 162–166. [CrossRef]
33. Cognard, G.; Ozouf, G.; Beauger, C.; Berthomé, G.; Riassetto, D.; Dubau, L.; Chattot, R.; Chatenet, M.; Maillard, F. Benefits and limitations of Pt nanoparticles supported on highly porous antimony-doped tin dioxide aerogel as alternative cathode material for proton-exchange membrane fuel cells. *Appl. Catal. B* **2017**, *201*, 381–390. [CrossRef]
34. Bagheri, S.; Julkapli, N.M.; Hamid, S.B.A. Titanium Dioxide as a Catalyst Support in Heterogeneous Catalysis. *Sci. World J.* **2014**, *2014*, 727496. [CrossRef]
35. Qu, W.; Wang, Z.; Sui, X.; Gu, D. An efficient antimony doped tin oxide and carbon nanotubes hybrid support of Pd catalyst for formic acid electrooxidation. *Int. J. Hydrog. Energy* **2014**, *39*, 5678–5688. [CrossRef]
36. Godoi, C.M.; Gutierrez, I.M.; Gomes, P.V.R.; Coelho, J.F.; Zambiazi, P.J.; Otubo, L.; Neto, A.O.; De Souza, R.F.B. Production of Methanol on PdCu A. T. O. in a Polymeric Electrolyte Reactor of the Fuel Cell Type from Methane. *Methane* **2022**, *10*, 218–230. [CrossRef]
37. Nandenha, J.; De Souza, R.F.B.; Assumpção, M.H.M.T.; Spinacé, E.V.; Neto, A.O. Preparation of PdAu/C-Sb2O5·SnO2 electrocatalysts by borohydride reduction process for direct formic acid fuel cell. *Ionics* **2013**, *19*, 1207–1213. [CrossRef]
38. Aragón, F.H.; Coaquira, J.A.H.; Hidalgo, P.; da Silva, S.W.; Brito, S.L.M.; Gouvêa, D.; Morais, P.C. Evidences of the evolution from solid solution to surface segregation in Ni-doped SnO_2 nanoparticles using Raman spectroscopy. *J. Raman Spectrosc.* **2011**, *42*, 1081–1086. [CrossRef]
39. Leonardy, A.; Hung, W.-Z.; Tsai, D.-S.; Chou, C.-C.; Huang, Y.-S. Structural Features of SnO_2 Nanowires and Raman Spectroscopy Analysis. *Cryst. Growth Des.* **2009**, *9*, 3958–3963. [CrossRef]
40. Muniz-Miranda, M.; Zoppi, A.; Muniz-Miranda, F.; Calisi, N. Palladium Oxide Nanoparticles: Preparation, Characterization and Catalytic Activity Evaluation. *Coatings* **2020**, *10*, 207. [CrossRef]
41. Yeo, B.S.; Klaus, S.L.; Ross, P.N.; Mathies, R.A.; Bell, A.T. Identification of Hydroperoxy Species as Reaction Intermediates in the Electrochemical Evolution of Oxygen on Gold. *ChemPhysChem* **2010**, *11*, 1854–1857. [CrossRef]
42. Yan, B.-X.; Zhu, Y.-Y.; Wei, Y.; Pei, H. Study on surface enhanced Raman scattering of Au and Au@Al_2O_3 spherical dimers based on 3D finite element method. *Sci. Rep.* **2021**, *11*, 8391. [CrossRef]
43. De Souza, R.F.B.; Neto, É.T.; Calegaro, M.L.; Santos, E.A.; Martinho, H.S.; Santos, M.C.D. Ethanol Electro-oxidation on Pt/C Electrocatalysts: An "In Situ" Raman Spectroelectrochemical Study. *Electrocatalysis* **2011**, *2*, 28–34. [CrossRef]
44. Nandenha, J.; Fontes, E.H.; Piasentin, R.M.; Fonseca, F.C.; Neto, A.O. Direct oxidation of methane at low temperature using Pt/C, Pd/C, Pt/C-ATO and Pd/C-ATO electrocatalysts prepared by sodium borohydride reduction process. *J. Fuel Chem. Technol.* **2018**, *46*, 1137–1145. [CrossRef]
45. Scarano, D.; Bertarione, S.; Spoto, G.; Zecchina, A.; Areán, C.O. FTIR spectroscopy of hydrogen, carbon monoxide, and methane adsorbed and co-adsorbed on zinc oxide. *Thin Solid Films* **2001**, *400*, 50–55. [CrossRef]

46. Hamada, K.; Morishita, H. The Rotation-Vibrational Spectra and Structures of Methanol and Acetonitrile. *Spectrosc. Lett.* **1980**, *13*, 15–29. [CrossRef]
47. Christensen, P.A.; Linares-Moya, D. The Role of Adsorbed Formate and Oxygen in the Oxidation of Methanol at a Polycrystalline Pt Electrode in 0.1 M KOH: An In Situ Fourier Transform Infrared Study. *J. Phys. Chem. C* **2010**, *114*, 1094–1101. [CrossRef]

Disclaimer/Publisher's Note: The statements, opinions and data contained in all publications are solely those of the individual author(s) and contributor(s) and not of MDPI and/or the editor(s). MDPI and/or the editor(s) disclaim responsibility for any injury to people or property resulting from any ideas, methods, instructions or products referred to in the content.